

Revisiting thermodynamics in (LiF, NaF, KF, CrF₂)-CrF₃ by first-principles calculations and CALPHAD modeling

Rushi Gong¹, Shun-Li Shang¹, Yi Wang¹, Jorge Paz Soldan Palma¹, Hojong Kim¹, and Zi-Kui Liu¹

¹Department of Materials Science and Engineering, The Pennsylvania State University, University Park, PA 16802, USA

Abstract

The thermodynamic description of the (LiF, NaF, KF, CrF₂)-CrF₃ systems has been revisited, aiming for a better understanding of the effects of Cr on the FLiNaK molten salt. First-principles calculations based on density functional theory (DFT) were performed to determine the electronic and structural properties of each compound, including the formation enthalpy, volume, and bulk modulus. DFT-based phonon calculations were carried out to determine the thermodynamic properties of compounds, for example, enthalpy, entropy, and heat capacity as functions of temperature. Phonon-based thermodynamic properties show a good agreement with experimental data of binary compounds LiF, NaF, KF, CrF₃, and CrF₂, establishing a solid foundation to determine thermodynamic properties of ternary compounds as well as to verify results estimated by the Neumann-Kopp rule. Additionally, DFT-based ab initio molecular dynamics (AIMD) simulations were employed to predict mixing enthalpies of liquid salts. Using DFT-based results and experimental data in the literature, the (LiF, NaF, KF, CrF₂)-CrF₃ system has been remodeled in terms of the CALculation of PHase Diagrams (CALPHAD) approach using the modified quasichemical model with quadruplet approximation (MQMQA) for liquid. Calculated phase stability in the present work shows an excellent agreement with experiments, indicating the effectiveness of combining DFT-based total energy, phonon, and AIMD calculations, and CALPHAD modeling to provide the thermodynamic description in complex molten salt systems.

Highlights

- Temperature-dependent thermodynamic properties of compounds in (LiF, NaF, KF, CrF₂)-CrF₃ predicted by DFT-based phonon calculations.
- Mixing enthalpies of liquid salts in (LiF, NaF, KF)-CrF₃ predicted by AIMD.
- The (LiF, NaF, KF, CrF₂)-CrF₃ system re-modeled with MQMQA to describe liquid.

Keywords: FLiNaK, Molten Salts, First-principles calculations, Phonon, AIMD, CALPHAD modeling

1 Introduction

Molten Salt Reactor (MSR) is one of the few game-changing concepts with rigorous safety standards while simultaneously achieving high levels of reliability and efficiency due to the use of liquid, instead of solid, fuel in the reactor [1–3]. The MSR concept consists of a molten salt mixture (such as $\text{LiF-BeF}_2\text{-UF}_4$), in which the fissile and fertile isotopes (such as ^{233}U , ^{235}U , ^{238}U , and/or ^{239}Pu) are dissolved, circulating from the reactor core to the heat exchanger continuously [1,4]. A very important feature of this system is its safety, requiring more attention to select molten salts [5]. Alkali and alkaline-earth metal fluorides, in which actinide fluorides (such as UF_4 and PuF_3) can be dissolved, are considered as the key materials for MSR fuel salts [1]. For example, the fuel salt of $^7\text{LiF-BeF}_2\text{-ZrF}_4\text{-UF}_4$ with ^{235}U , ^{233}U , and/or ^{239}Pu as the fissile driver was used in the Molten Salt Reactor Experiment (MSRE) operated at Oak Ridge National Laboratory (ORNL) from 1965 to 1969 [1] with the coolant salt in the secondary loop being $^7\text{Li}_2\text{BeF}_4$. The Molten Salt Chemistry Workshop [1] suggested that fluoride salts, which are similar to the MSRE salts, are primarily for the thermal spectrum applications and for the primary and secondary coolant candidates, such as the FLiNaK, i.e., the LiF-NaF-KF eutectics with its mole fraction around 0.465-0.115-0.420 [6,7].

Chromium (Cr) is one of the key elements in current reference structural materials for fluoride salt reactors, for example, the Hastelloy-N as the container material (72%Ni-16%Mo-7%Cr-5%Fe in wt.%) [8,9]. In the fluoride salt environment, Cr in Ni-based alloy is more susceptible to corrosion compared to other metal elements [10–12]. For example, Olson et al. [10] performed corrosion tests on a number of Ni-based alloys with different Cr alloying contents. They showed the

dissolution of Cr into molten salt and correlated the relationship between Cr content and corrosion resistance [10]. Ouyang et al. [11] investigated the corrosion behavior of Hastelloy-N in FLiNaK after 100-1000 h at 700 °C, and the aggregate dissolution of Cr was observed. Recently, Liu et al. [12] studied Hastelloy-N and showed that the corrosion rate of Cr in FLiNaK-CrF₃ is higher than that in FLiBe-CrF₃ with Cr³⁺ as the product. Thus, it is important to investigate solubility and multivariate distribution patterns of Cr in FLiNaK. There exists extensive thermodynamic modeling work related to the LiF-NaF-KF system, several studies, including those by Chartrand and Pelton [13], Wang et al. [14], and Ard et al. (MSTDB-TC database) [15] have explored this system using thermodynamic modeling. However, we noticed that thermodynamic modeling of the FLiNaK-CrF₃ system has been performed based on incomplete and empirically estimated thermochemical data by Yin et al. [16,17] and Dumaire et al. [18] (see Sec. 2.1). A comprehensive study on thermodynamic properties of all solid and liquid phases in FLiNaK-CrF₃ is yet to be conducted.

In the present work, the thermodynamic description of the (LiF, NaF, KF, CrF₂)-CrF₃ system is re-modeled using the CALPHAD (CALculation of PHAse Diagram) approach [19–21] with experimental data in the literature, and thermochemical data from the present density functional theory (DFT) based first-principles calculations, phonon calculations, and ab initio molecular dynamics (AIMD) simulations. In particular, the modified quasichemical model with quadruplet approximation (MQMQA) [22] is adopted for the liquid phase. The open-source software ESPEI (Extensible Self-optimizing Phase Equilibria Infrastructure) [23,24] with the computational engine

of PyCalphad [25,26] is used for the present CALPHAD modeling. A comprehensive description of thermodynamic properties in the (LiF, NaF, KF, CrF₂)-CrF₃ system is achieved and compared well with experimental data in the literature.

2 Literature review of thermodynamic properties

2.1 Thermochemical data

The (LiF, NaF, KF, CrF₂)-CrF₃ system includes five binary (endmember) compounds, i.e., LiF, NaF, KF, CrF₃ and CrF₂, and eight ternary (intermetallic) compounds, i.e., Li₃CrF₆, Na₃CrF₆, Na₅Cr₃F₁₄, NaCrF₄, K₃CrF₆, K₂CrF₅, KCrF₄, and K₂Cr₅F₁₇. These ternary compounds were first suggested by De Kozak [27] and confirmed by structural studies [28–35] via the X-ray diffraction (XRD) method, which was summarized by Dumaire et al. [18]. However, thermochemical data of these compounds are scarce. Yin et al. [16,17,36] performed DFT calculations at 0 K to determine the formation enthalpies of Li₃CrF₆, Na₃CrF₆, Na₅Cr₃F₁₄, NaCrF₄, and KCrF₄. Dumaire et al. [18] estimated the heat capacities of these compounds based on the Neumann-Kopp rule in terms of the compositional average of heat capacity values of the corresponding compounds or elements [37]. For the liquid phase, experimental data such as mixing enthalpy are not available in the AF-CrF₃ (A=Li, Na, and K) systems. Instead, Yin et al. [16,17,36] applied an empirical model to estimate the mixing enthalpy of liquid from the parameters of ions such as ionic radius.

2.2 Phase equilibrium data

Phase equilibria in the LiF-CrF₃, NaF-CrF₃, and KF-CrF₃ binary systems were investigated by De Kozak [27,28] using differential thermal analysis (DTA). In LiF-CrF₃, two eutectic reactions were measured, i.e., Liquid \leftrightarrow LiF + Li₃CrF₆ at 1003 K and around mole fraction X(CrF₃) = 0.15 and Liquid \leftrightarrow CrF₃ + Li₃CrF₆ at 1059 K and X(CrF₃) = 0.35. In NaF-CrF₃, one peritectic reaction of Liquid + CrF₃ \leftrightarrow NaCrF₄ at 1234 K and three eutectic reactions were determined, i.e., Liquid \leftrightarrow NaCrF₄ + Na₅Cr₃F₁₄ at 1133 K, Liquid \leftrightarrow Na₃CrF₆ + Na₅Cr₃F₁₄ at 1143 K, and Liquid \leftrightarrow Na₃CrF₆ + NaF at 1166 K and around X(CrF₃) = 0.123. In KF-CrF₃, De Kozak [27,28] reported three peritectic reactions and two eutectic reactions, i.e., Liquid + CrF₃ \leftrightarrow K₂Cr₅F₁₇ at 1390 K, Liquid + K₃CrF₆ \leftrightarrow K₂CrF₅ at 1133 K, and Liquid + K₂Cr₅F₁₇ \leftrightarrow KCrF₄ at 1200 K, and Liquid \leftrightarrow K₃CrF₆ + KF at 1115 K and around X(CrF₃) = 0.048, and Liquid \leftrightarrow K₂CrF₅ + KCrF₄ at 1112 K and around X(CrF₃) = 0.45. Sturm [30] reported phase equilibria in CrF₂-CrF₃ via quenching experiments and suggested one solid solution phase in CrF₂-CrF₃ with composition of CrF₃ between 0.42 and 0.46 (near Cr₂F₅). However, the stability of this Cr₂F₅ solid solution phase was not explored in temperatures below 1023 K. The melting point of Cr₂F₅ was determined to be around 1270 K [30]. Sturm [30] reported one eutectic reaction, Liquid \leftrightarrow CrF₂ + Cr₂F₅ at 1103 K around X(CrF₃) = 0.14, and one peritectic reaction Liquid + CrF₃ \leftrightarrow Cr₂F₅ at 1272 K around X(CrF₃) = 0.29. Two solid solution phases near the endmembers CrF₃ and CrF₂ were identified from X(CrF₃) = 0~0.01 and from X(CrF₃) = 0.90 ~1, respectively.

3 Methodology

3.1 DFT-based first-principles calculations

3.1.1 Helmholtz energy at finite temperatures

The Helmholtz energy $F(V, T)$ as a function of volume (V) and temperature (T) in terms of the DFT-based quasiharmonic approximation (QHA) can be determined by [38],

$$F(V, T) = E(V) + F_{el}(V, T) + F_{vib}(V, T) \quad \text{Eq. 1}$$

where the first term $E(V)$ is static energy at 0 K without the zero-point vibrational energy. In the present work, a four-parameter Birch-Murnaghan (BM4) equation of state (EOS) [38] as shown in **Eq. 2** was used to obtain equilibrium properties at zero external pressure ($P = 0$ GPa), including the static energy E_0 , volume (V_0), bulk modulus (B_0) and its pressure derivate (B').

$$E(V) = a + bV^{-2/3} + cV^{-4/3} + dV^{-2} \quad \text{Eq. 2}$$

where a , b , c , and d are fitting parameters. The second term in **Eq. 1**, $F_{el}(V, T)$, represents the temperature-dependent thermal electronic contribution [39],

$$F_{el}(V, T) = E_{el}(V, T) - T \cdot S_{el}(V, T) \quad \text{Eq. 3}$$

where E_{el} and S_{el} are the internal energy and entropy of thermal electron excitations, respectively, which can be obtained by electronic density of states (DOS). Note that the thermal electronic contribution to Helmholtz free energy is negligible for non-metal, considering the Fermi level lies in the band gap. The third term in **Eq. 4**, $F_{vib}(V, T)$, represents the vibrational contribution [39,40],

$$F_{vib}(V, T) = k_B T \sum_q \sum_j \ln \left\{ 2 \sinh \left[\frac{\hbar \omega_j(q, V)}{2k_B T} \right] \right\} \quad \text{Eq. 5}$$

where $\omega_j(q, V)$ represents the frequency of the j^{th} phonon mode at wave vector q and volume V , and \hbar the reduced Plank constant.

3.1.2 Details of first-principles calculations

All DFT-based first-principles and phonon calculations in the present work were performed by the Vienna *Ab initio* Simulation Package (VASP) [41]. The projector augmented-wave method (PAW) was used to account for electron-ion interactions in order to increase computational efficiency compared with the full potential methods [42,43]. Electron exchange and correlation effects were described using both the local density approximation (LDA) [44] and the generalized gradient approximation (GGA) as implemented by Perdew, Burke, and Ernzerhof (PBE) [45]. In addition, the DFT+U approach was employed for 11 compounds containing Cr, i.e., CrF₂, CrF₃, Cr₂F₅, Li₃CrF₆, Na₃CrF₆, Na₅Cr₃F₁₄, NaCrF₄, K₃CrF₆, K₂CrF₅, KCrF₄, K₂Cr₅F₁₇. The effective U values for Cr were selected as 3.7 eV, considering 3 ~ 4eV was commonly used in the literature [46–48]. The spin configurations were also considered for these 11 compounds containing Cr. All possible configurations by varying spin up and spin down of Cr atoms were explored by the ATAT code [49]. The spin configuration with the lowest energy for each Cr-containing compound was used for DFT and phonon calculations.

In the present work, DFT-based first-principles and phonon calculations were performed by using the open-source software DFTTK [50]. Using DFTTK, structure information is the only required input, then robust relaxation schemes can be automatically performed to obtain equilibrium results at 0 K and thermodynamic properties at finite temperatures through the QHA. During DFTTK calculations, the plane-wave cutoff energy was set as 520 eV. Table 1 lists the k-points meshes for DFT-based total energy calculations, the supercell sizes, and the k-points meshes for phonon calculations. The phonon DOS and force constants were analyzed using the YPHON code [51], which has been integrated into DFTTK [50].

3.2 AIMD simulations

The *ab initio* molecular dynamics (AIMD) simulations in the present work were also performed by VASP [41]. The supercells containing 108 or 128 atoms with periodic boundary were used for at least six different compositions in the AF-CrF₃ (A= Li, Na, and K) systems, including A₆₄F₆₄, A₄₂Cr₆F₆₀, A₃₆Cr₉F₆₃, A₃₂Cr₁₆F₈₀, A₁₈Cr₁₈F₇₂, A₁₆Cr₂₄F₈₈, A₁₀Cr₂₂F₇₆, and Cr₃₂F₉₆ (A=Li, Na, and K). The NVT canonical ensemble (i.e., the fixed number of atoms N, volume V, and temperature T) with a Nosé thermostat for temperature control [52] were employed in the present work. The temperature for each supercell was set as 1700 K, which is above all the temperatures of liquidus in the AF-CrF₃ (A= Li, Na, and K) systems. A single Γ point $1 \times 1 \times 1$ was used as the k-point mesh, together with a 400 eV cutoff energy. During AIMD simulations, the Newton's equation of motion was solved via the Verlet algorithm with a time step of 2 fs and each calculation is run for 10,000 steps to reach thermal equilibrium.

3.3 CALPHAD modeling

In the present work, the compounds and endmembers in the AF-CrF₃ (A=Li, Na, and K) systems are treated as stoichiometric compounds, including four binary endmembers, i.e., LiF, NaF, KF, and CrF₃, and eight ternary compounds, i.e., Li₃CrF₆, Na₃CrF₆, Na₅Cr₃F₁₄, NaCrF₄, K₃CrF₆, K₂CrF₅, KCrF₄, and K₂Cr₅F₁₇ (as listed in Sec.2.1). Thermodynamic functions of the binary endmembers are taken from the JRC database [53], JANAF tables [54], IVTAN tables [55], and SSUB database [56]. The Gibbs energy can be expressed as

$$G_m = \Delta_f H_m^0(298.15) - T S_m^0(298.15) + \int_{298.15}^T C_{P,m} dT - T \int_{298.15}^T \frac{C_{P,m}}{T} dT \quad \text{Eq. 6}$$

where $\Delta_f H_m^0(298.15)$ is the standard formation enthalpy, $S_m^0(298.15)$ the standard entropy at 298.15 K, and $C_{P,m}$ the heat capacity. For ternary compounds, their thermodynamic data including enthalpy, entropy, and heat capacity are obtained through DFT-based first-principles and phonon calculations, which are presented in Sec. 4.1.

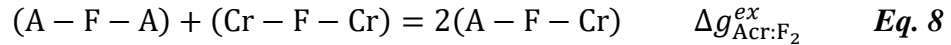
The MQMQA [57,58] is used to describe the liquid phase by considering the short-range ordering (SRO) occurred in liquid salts. Within the MQMQA, two sublattices which separate the cations from the anions are introduced to form quadruplets and account for the first nearest neighbors (FNN) and the second nearest neighbors (SNN) interactions. Here, the model (A, Cr)(F) is

introduced and hence the AA/FF, CrCr/FF, and ACr/FF quadruplets (A=Li, Na, and K) are formed to consider the interactions among them. Coordination numbers Z are defined to describe the quadruplets. Z of anions can be calculated from **Eq. 7** to maintain charge neutrality as follows

$$\frac{q_A}{Z_{AB:FF}^A} + \frac{q_B}{Z_{AB:FF}^B} = 2 \times \frac{q_F}{Z_{AB:FF}^F} \quad \text{Eq. 7}$$

where q_i is the charges of ion i (= Li, Na, K, Cr, or F). Coordination numbers used in the present work are shown in Table 2.

The excess Gibbs energy G^{excess} relates to the formation Gibbs energy of the quadruplet, $\Delta g_{quadruplet}^{ex}$, by considering the following reaction,



where $\Delta g_{Acr:F_2}^{ex}$ represents the Gibbs energy change when forming the quadruplet and can be described by

$$\Delta g_{Acr:F_2}^{ex} = \sum_{i \geq 0, j \geq 0} g_{Acr:F_2}^{ij} \chi_{Acr:F_2}^i \chi_{CrA:F_2}^j \quad \text{Eq. 9}$$

where $g_{Acr:F_2}^{ij}$ is a function of temperature and it is independent of composition. $\chi_{Acr:F_2}^i$ and $\chi_{CrA:F_2}^j$ are composition-dependent terms,

$$\chi_{\text{Acr:F}} = \frac{n_{\text{AA:F}}}{n_{\text{Acr:F}} + n_{\text{AA:F}} + n_{\text{CrCr:F}}} \quad \text{Eq. 10}$$

where $n_{\text{Acr:F}}$ is the moles of (A – F – Cr) shown in **Eq. 10**.

In the $\text{CrF}_2\text{-CrF}_3$ system, there are three solid solution phases, i.e., CrF_2 near the Cr-rich region, CrF_3 near the F-rich region, and Cr_2F_5 showing on the middle region of the $\text{CrF}_2 - \text{CrF}_3$ phase diagram. The present work adopts the same models used by Dumaire et al. [18], where the regular solution model with the Kohler-Toop interpolation [59–62] is used for Cr_2F_5 . For solid solution phases near CrF_2 and CrF_3 , the sublattice model is used for each phase, respectively, considering the Wyckoff positions of CrF_2 and CrF_3 as follows. CrF_2 possesses the symmetry with space group $\text{P2}_1/\text{c}$ with two Wyckoff sites of 2a and 4e, and the sublattice model $(\text{Cr}, \text{Va})_1(\text{F}, \text{Va})_2$ is hence used with Va representing the vacancy. CrF_3 phase is modeled by $(\text{Cr}, \text{Va})_1(\text{F}, \text{Va})_3$ by considering its space group $\text{R}\bar{3}\text{c}$ and the two Wyckoff sites of 2b and 6e. The Gibbs energy per mole of xxx is formulated as:

$$G_m = \sum_{i=\text{Cr,Va}} \sum_{j=\text{F,Va}} y'_i y''_j {}^oG_{i:j} + RT \left(\sum_{i=\text{Cr,Va}} y'_i \ln(y'_i) + \sum_{j=\text{F,Va}} y''_j \ln(y''_j) \right) \quad \text{Eq. 11}$$

$$+ y'_{\text{Cr}} y'_{\text{Va}} (y''_{\text{F}} L_{\text{Cr,Va:F}}) + y''_{\text{F}} y''_{\text{Va}} (y'_{\text{Cr}} L_{\text{Cr:F,Va}})$$

where $y_i^{(s)}$ is the site fraction of component i on sublattice s , ${}^oG_{i:j}$ the Gibbs energy of the endmember ($i:j$), and L the interaction parameters which can be expanded using the Redlich-Kister polynomials [63].

Machine learning (ML) was used to estimate more phase equilibria data in terms of a graphic neural network model developed by Hong et al. [64] to predict melting points of compounds with composition as input. Melting temperatures of the present ternary compounds including Li_3CrF_6 , Na_3CrF_6 , $\text{Na}_5\text{Cr}_3\text{F}_{14}$, NaCrF_4 , K_3CrF_6 , K_2CrF_5 , KCrF_4 , and $\text{K}_2\text{Cr}_5\text{F}_{17}$ are estimated by this ML model [64].

Thermodynamic modeling of the (LiF, NaF, KF, CrF_2)- CrF_3 system was carried out by means of the open-source software ESPEI [23], which uses PyCalphad [25] as computational engine for thermodynamic calculations with the newly implemented MQMQA [65]. All model parameters were simultaneously optimized through the Bayesian approach using the Markov Chain Monte Carlo (MCMC) method [23]. The input data were primarily experimental phase equilibrium data including two or more co-existing phases. For stoichiometric compounds, their thermochemical data from DFT-based calculations were also used as input. For the liquid phase, its mixing enthalpy from AIMD calculations was used as input for refining model parameters. In the present work, each model parameter employed two Markov chains with a standard derivation of 0.1 when initializing its Gaussian distribution. During the modeling process, the chain values can be tracked and the MCMC processes were performed until the model parameters converged.

4 Results and discussion

4.1 Thermodynamic properties in (LiF, NaF, KF, CrF₂)-CrF₃ by first-principles calculations

Table 3 shows the predicted equilibrium properties of V_0 , B_0 , and B' by the EOS E-V fitting at 0 K in comparison with experimental bulk moduli [66–71]. The B_0 results from GGA show a good agreement with experimental measurements. For the LiF compound, GGA predicts $B_0 = 67.6$ GPa and $B' = 4.17$, aligning well with the measured values of 65.4 GPa and 4.98 by Boehler et al. [68]. In comparison with the three measured B_0 values of 66.5 GPa by Yagi [66], 76.9 GPa by Haussühl [67], and 65.4 GPa by Boehler et al. [68], the B_0 result by GGA shows a mean absolute error (MAE) of 4.2 GPa, while LDA predicts $B_0 = 86.5$ GPa with a higher MAE of 16.9 GPa. Considering the NaF compound, GGA predicts $B_0 = 45.0$ GPa, matching with the measured 45.9 GPa by Yagi [66] but lower than the measured values of 53.8 GPa by Haussühl [67], 52.3 GPa Rao [69], and 48.2 GPa Bensch et al. [70] with the MAE around 5 GPa. On the other hand, LDA predicts $B_0 = 61.4$ GPa, which is higher than the experimental B_0 [66,67,69,70] with MAE = 11.4 GPa. Additionally, for the B' values of NaF, LDA predicts $B' = 4.74$, which is higher than the predicted 4.60 by GGA and closer to 5.89 reported by Bensch et al. [70]. Regarding the KF compound, the measured B_0 values (37.0 GPa by Yagi [66] and 35.5 GPa by Haussühl [67]) fall between the LDA result of 43.5 GPa and the GGA result of 28.9 GPa. The MAE value of LDA with respect to the measured B_0 values is 7.25 GPa, slightly lower than MAE = 7.35 GPa by GGA. As for the CrF₃ compound, GGA+U reports $B_0 = 29.3$ GPa, showing a 0.3% difference compared to 29.2 GPa measured by Jørgensen et al. [71]. LDA+U predicts $B_0 = 46.2$ GPa, which is 58% higher than the measured 29.2 GPa [71]. The present results indicate that LDA predicts smaller V_0

and higher B_0 values than those from GGA. It is consistent with the previous observations that LDA tends to underestimate lattice constants and overestimate cohesive energy with respect to GGA [72,73].

Figure 1 compares the phonon DOS of LiF, NaF, and KF obtained using LDA and GGA in comparison with direct measurements by neutron scattering [74,75] or fittings in terms of measurements [76]. Overall, the peak positions of the experimental phonon DOS are well reproduced by both LDA and GGA. However, in the low-frequency region (e.g., $< 5\text{THz}$ for LiF and NaF, and $< 3\text{THz}$ for KF), the phonon DOS predicted by LDA show a better match in both the shape and the peak position with respect to experimental data [74–76] than those from GGA. This observation suggests that LDA predicts more reliable thermodynamic properties of LiF, NaF, and KF when employing the phonon based QHA, since these properties are mainly regulated by phonon DOS at low frequency regions [77].

Figure 2 illustrates a comparison of the predicted heat capacity (C_p), entropy (S), and enthalpy (H_{300}) of LiF, NaF, and KF in terms of the phonon-based QHA, where the DFT calculations were conducted using both the LDA and GGA, and the predicted results are compared to the data from the SSUB database [56]. In general, thermodynamic properties predicted by LDA align well with the results from SSUB. The most substantial difference between LDA and SSUB is the C_p values of KF, where a 6% disparity is noted. Furthermore, these comparisons reveal that the LDA results

exhibit a better agreement with SSUB than the GGA results, particularly for LiF. For example at 1100 K, the C_p values predicted by LDA demonstrate only a 2% difference compared to those from the SSUB [56], whereas an 18% difference is observed when using GGA. Figure 2 indicates that the QHA in terms of LDA yields more reliable predictions of thermodynamic properties in LiF-NaF-KF-based system, agreeing with the observations in phonon DOS in Figure 1. Subsequent DFT calculations were hence performed using the LDA approach.

Figure 3 shows the present DFT predictions and the values in SSUB [56] regarding C_p , S , and $H-H_{300}$ for CrF_3 and CrF_2 . In general, the present predictions tend to be lower than those obtained from SSUB [56]. For CrF_3 , the DFT predicted $C_p = 19.77$ J/mol-atom-K closely aligns with the SSUB value of 19.73 J/mol-atom-K at 300 K. As the temperature increases to 1300 K, the difference increases to 9%. Similarly, for CrF_2 , the $C_p = 21.22$ J/mol-atom-K at 300 K by DFT is in good agreement with the value of 21.66 from SSUB. At a higher temperature of 1140 K, the difference expands to 12%. Regarding entropy, DFT predicts lower S values for both CrF_3 and CrF_2 than those in SSUB across the temperature range shown in Figure 3. At high temperatures (e.g., 1600 K for CrF_3 and 1140 K for CrF_2), it shows a 10% difference in CrF_3 and 14% in CrF_2 . It is found that a good agreement is observed regarding $H-H_{300}$ values of CrF_3 and CrF_2 between the DFT calculations and the SSUB at lower temperatures (< 1000 K for CrF_3 and < 600 K for CrF_2). $H-H_{300}$ from DFT becomes slightly lower than that in SSUB [56] with increasing temperature, with the differences, for example, around 5% in CrF_3 at 1650 K and 9% in CrF_2 at 1140 K.

DFT calculations of the aforementioned LiF, NaF, KF, and CrF₃ are used as the reference states to describe thermodynamic properties of the nine ternary compounds of Li₃CrF₆, Na₃CrF₆, Na₅Cr₃F₁₄, NaCrF₄, K₃CrF₆, K₂CrF₅, KCrF₄, K₂Cr₅F₁₇, and Cr₂F₅. Table 5 shows the present DFT values of formation enthalpy ($\Delta_f H_m$) of these ternary compounds using the LDA+U approach, together with the reactions to form these compounds. Table 5 shows that the $\Delta_f H_m$ values are negative for all ternary compounds with reference to their corresponding binary compounds. Yin et al. [16,36] conducted DFT calculations for Li₃CrF₆ and Na₃CrF₆. Predicted $\Delta_f H_m$ values from the Materials Project [78] and the Open Quantum Materials Database (OQMD) [79] are also listed in Table 5 and displayed in Figure 4. The present DFT calculations by LDA+U predict higher $\Delta_f H_m$ values of Li₃CrF₆ and Na₃CrF₆ than those by Yin et al. [16,36] using GGA. The present DFT calculations align better with results from the Materials Project [78] and OQMD [79] than calculations from Yin et al. [16,36]. Figure 4 displays the convex hulls for the LiF-CrF₃, NaF-CrF₃, and KF-CrF₃ systems based on the $\Delta_f H_m$ values listed in Table 5. These convex hulls serve as indicators regarding the stability of ternary compounds in these systems. Li₃CrF₆ is on the convex hull, suggesting that it is stable in the LiF-CrF₃ system. In the NaF-CrF₃ system, Na₃CrF₆ is located on the hull, indicating its stability at 0 K. Na₅Cr₃F₁₄ shows an elevation of 1.09 kJ/mol-atom above the hull, and NaCrF₄ shows 0.42 kJ/mol-atom above hull. In the KF-CrF₃ system, K₂CrF₅ is on the convex hull at 0 K. K₂Cr₅F₁₇ is the farthest away from the convex hull (1.31 kJ/mol-atom above it), while K₃CrF₆ and KCrF₄ are 0.62 kJ/mol-atom and 0.61 kJ/mol-atom above the hull, respectively. These calculations at 0 K suggests that Na₅Cr₃F₁₄, NaCrF₄, K₂Cr₅F₁₇,

K_3CrF_6 , and KCrF_4 are not stable at 0 K, while De Kozak [27] reported the existence of above ternary compounds at high temperature. It suggests that phonon-based QHA is necessary to investigate the thermodynamic properties of ternary compounds at high temperatures.

Figure 5 shows the predicted heat capacities C_p of ternary compounds in the AF-CrF_3 ($A = \text{Li, Na, and K}$) systems from the phonon-based QHA, in comparison with the results estimated by the Neumann-Kopp rule [37], which were used in CALPHAD modeling by Dumaire et al. [18]. It shows that the Neumann-Kopp rule gives a good match with results by phonon-based QHA in the LiF-CrF_3 system. However, in the NaF-CrF_3 and KF-CrF_3 systems, the Neumann-Kopp rule estimates higher values of C_p with respect to the values predicted by phonon-based QHA. The differences between the LiF-CrF_3 system and the NaF/KF-CrF_3 may be attributed to variations in melting temperatures between ternary and corresponding binary compounds. For example, in the LiF-CrF_3 system, the melting temperature of Li_3CrF_6 is reported at 1129 K [27], which is close to that of LiF at 1121 K [56] and below that of CrF_3 at 1698 K [56]. Considering the temperature below the melting point of Li_3CrF_6 ($T < 1129$ K), there are reliable resources of C_p data from two endmembers LiF and CrF_3 , thus the Neumann-Kopp rule C_p estimation of Li_3CrF_6 is acceptable. However, in the NaF-CrF_3 system, Na_3CrF_6 melts at 1413 K [27], while NaF melts at 1269 K [56], indicating that there is an approximately 150 K temperature range without reliable C_p data for NaF . In contrast, the phonon-based calculations are direct predictions of ternary compounds and it provides more accurate descriptions of thermodynamic properties for compounds than those by the Neumann-Kopp rule used by Dumaire et al. [18], especially at high temperatures. Therefore,

the phonon-based QHA results were used in the present CALPHAD modeling to improve the accuracy in describing ternary compounds. Note that the C_p values for compounds in the (LiF, NaF, KF, and CrF_2)- CrF_3 systems can be predicted using the Supplementary XML file.

4.2 Thermodynamic modeling

Figure 6 shows the phase diagrams of the (LiF, NaF, KF, and CrF_2)- CrF_3 systems calculated from present models and compared with experimental data by De Kozak [27,28] and Sturm [30]. The present CALPHAD modeling shows a good agreement regarding phase boundaries with experimental data. As an example, Table 4 summarizes the presently modeled parameters for liquid, while the complete thermodynamic database can be found in the Supplementary XML file. Details of the invariant reactions and the congruent melting temperature calculated from the present modeling work compared to experiments [27,28,30] and ML predictions using Hong et al.'s model [64] are listed in Table 6 with discussion below.

In the LiF- CrF_3 system, the present prediction of the eutectic reaction $\text{Liquid} \leftrightarrow \text{LiF} + \text{Li}_3\text{CrF}_6$ at $x(\text{CrF}_3) = 0.159$ and $T = 1004$ K matches well with experimental values of $x(\text{CrF}_3) = 0.150$ and $T = 1003$ K [27]. The largest difference is observed for $\text{Liquid} \leftrightarrow \text{CrF}_3 + \text{Li}_3\text{CrF}_6$, with eutectic temperature of 1051 K from the present modeling, which is 8 K lower than the 1059 K reported by De Kozak [27]. The eutectic composition for this reaction at $x(\text{CrF}_3) = 0.345$ is notably improved from the 0.363 by Dumaire et al. [18] in comparison with the measured value 0.350 by

De Kozak [27]. The present prediction of congruent melting temperature (1134 K) is 5 K higher than experiment (1129 K by De Kozak) [27], improved from the prediction (1111 K) by Dumaire et al. [18].

In the NaF-CrF₃ system, the present modeling gives good predictions of eutectic and peritectic temperatures compared with experiments [27] with the largest difference of 3 K observed for Liquid + CrF₃ ↔ NaCrF₄ (1231 K from the present work and 1234 K by De Kozak [27]). The eutectic composition for the reaction Liquid ↔ NaF + Na₃CrF₆ is $x(\text{CrF}_3) = 0.093$, which is around 0.03 away from the experimental value $x(\text{CrF}_3) = 0.123$ [27]. The eutectic temperature for this reaction by the present modeling is 1164 K, whereas it is 1175 K modelled by Dumaire et al. [18]. In comparison to experimental value of 1166 K by De Kozak [27], the difference reduces from 9 K to 2 K. The present congruent melting temperature of Na₃CrF₆ is predicted at 1403 K, improving from the predicted 1385 K by Dumaire et al. [18] but slightly lower than experimental value of 1413 K [27]. For the two eutectic reactions without experimental data, i.e., Liquid ↔ Na₅Cr₃F₁₄ + Na₃CrF₆ and Liquid ↔ Na₅Cr₃F₁₄ + NaCrF₄, the present modeling provides similar predictions ($x(\text{CrF}_3) = 0.373$, $T = 1139$ K; $x(\text{CrF}_3) = 0.378$, $T = 1144$ K respectively) compared to those modeled by Dumaire et al. [18] ($x(\text{CrF}_3) = 0.371$, $T = 1145$ K; $x(\text{CrF}_3) = 0.383$, $T = 1144$ K, respectively).

In the KF-CrF₃ system, the present modeling work predicts the congruent melting of K₃CrF₆ at 1555 K, which is in good agreement with the experimental value of 1553 K [27]. For the eutectic reaction, Liquid \leftrightarrow KCrF₄ + K₂CrF₅, the present modeling predicts $x(\text{CrF}_3) = 0.408$ and $T = 1103$ K, whereas the values are $x(\text{CrF}_3) = 0.45$ and $T = 1112$ K modeled by De Kozak [27]. The present modeling improves the prediction of eutectic temperature of Liquid \leftrightarrow KF + K₃CrF₆ to 1110 K from the predicted 1108 K by Dumaire et al. [18], compared experimental value of 1115 K by De Kozak [27]. For the three peritectic reactions in the KF-CrF₃ system, the present modeling work predicts 1141 K for Liquid + K₃CrF₆ \leftrightarrow K₂CrF₅, 1194 K for Liquid + K₂Cr₅F₁₇ \leftrightarrow KCrF₄, and 1394 K for Liquid + CrF₃ \leftrightarrow K₂Cr₅F₁₇. These temperatures are comparable to 1133 K, 1200 K, and 1390 K, respectively, as measured by De Kozak [27], showing an MAE of 6 K.

In the CrF₂-CrF₃ system, the present modeling work improves the predicted invariant compositions. For the eutectic reaction Liquid \leftrightarrow CrF₂ + Cr₂F₅, the present work predicts the eutectic point at $x(\text{CrF}_3) = 0.124$. This value is higher than $x(\text{CrF}_3) = 0.115$ by Dumaire et al. [18] but aligns more closely with the experimental value $x(\text{CrF}_3) = 0.14$ by Sturm [30]. The eutectic temperature for this reaction is 1101 K predicted by the present modeling, which remains close to experimental 1103 K by Sturm [30]. For the peritectic reaction Liquid + CrF₃ \leftrightarrow Cr₂F₅, the present work predicts $x(\text{CrF}_3) = 0.299$ compared to measured $x(\text{CrF}_3) = 0.29$ by Sturm [30]. The present invariant temperature is predicted at 1276 K, demonstrating a slightly higher value by 4 K than the measured 1272 K by Sturm [30]. In the present work, the single-phase region of the Cr₂F₅ solid solution phase ranges from $x(\text{CrF}_3) = 0.38$ to $x(\text{CrF}_3) = 0.46$. This range aligns better with the

suggested values of $x(\text{CrF}_3)$ from 0.40 to 0.45 by Sturm [30], than $x(\text{CrF}_3)$ from 0.382 to 0.45 by Dumaire et al.[18]. Overall, by incorporating thermodynamic data of compounds by the present DFT calculations, the present modeling work yields improved predictions of phase diagrams.

In addition, the present CALPHAD modeling work implements the mixing enthalpy of liquid at 1700 K, which was obtained by the present AIMD simulations as described in Sec.3.2. Figure 7 shows the mixing enthalpy of liquid at 1700 K by AIMD at different compositions compared to the present modeling results and results by Dumaire et al. [18]. It clearly shows that the mixing enthalpy of liquid (dot-dashed lines) by Dumaire et al.'s modeling [18] is much less negative compared to the present AIMD calculations. For example, in the LiF-CrF₃ system at $x(\text{CrF}_3) = 0.2$, AIMD predicts the mixing enthalpy of -20.60 kJ/mol-atom at 1700 K, while Dumaire et al.'s modeling [18] shows -12.65 kJ/mol-atom, representing a 39% higher value. Using the present AIMD data of liquid for modeling, the present modeling work (solid lines) shows a great improvement. The present modeling work improves the prediction to -20.13 kJ/mol-atom at $x(\text{CrF}_3) = 0.2$ for the LiF-CrF₃ system. The differences between the AIMD results and Dumaire et al.'s work [18] are more pronounced in the NaF-CrF₃ and KF-CrF₃ systems. In the NaF-CrF₃ system, at $x(\text{CrF}_3) = 0.333$ (a composition region near the lowest mixing enthalpy), Dumaire et al.'s modeling [18] shows the mixing enthalpy of -25.45 kJ/mol-atom, while our modeling predicts -45.68 kJ/mol-atom. At the same condition, AIMD gives the mixing enthalpy of -47.37 kJ/mol-atom, which is about 22 kJ/mol-atom lower than Dumaire et al.'s results [18]. In the KF-CrF₃ system at $x(\text{CrF}_3) = 0.333$, Dumaire et al. [18] predicts -30.58 kJ/mol-atom, significantly higher

than -50.20 kJ/mol-atom by AIMD. The present modeling predicts -47.41 kJ/mol-atom, reducing the difference from the above mentioned 39% to the present 6%. It highlights that the present AIMD simulations enhances the reliability of the present modeling in describing liquid compared to the previous work [18]. The mixing enthalpy (dotted lines) modeling by Yin et al. [16] in the NaF-CrF₃ and KF-CrF₃ systems agree well with the results by the present modeling. Near the low mixing enthalpy region $x(\text{CrF}_3) = 0.333$ in the NaF-CrF₃ system, Yin et al. [16] suggests the mixing enthalpy of -40.54 kJ/atom, which is 10% higher than -45.68 kJ/atom from the present work. Note that Yin et al. [16] used an empirical model proposed by Robelin and Chartrand [80] to estimate the mixing enthalpy in liquid. Overall, the present modeling work has improved the predictions of liquid than the modeling works by Dumaire et al. [18] and Yin et al. [16].

In Yin et al.'s modeling work [16], the associate model was used to describe the liquid phase. This model was applied to describe the short-range ordering (SRO) by assuming 'associates', such as K₃CrF₆ and Na₃CrF₆ associates. This kind of assumption may cause issues when extrapolation into higher order systems [81]. In the present work, the MQMQA was employed to describe liquid and provides information of the first and the second nearest neighbors in complex liquid. As an example, Figure 8 shows the predicted fraction of each quadruplet in the liquid phase. The composition where the peak fraction of the ACr/FF (A=Li, Na, and K) quadruplets appears, indicates the SRO. In the LiF-CrF₃ system, the peak fraction of LiCr/FF with strong SRO is around $x(\text{CrF}_3) = 0.25$, which is consistent with the lowest mixing enthalpy around the $x(\text{CrF}_3) = 0.25$ as shown in Figure 7. In addition, Figure 8 presents the quadruplet fractions and the neighboring

environments of ions in liquid, which are difficult to obtain from the associate model due to its focus on associate clusters.

5 Conclusions

The present work revisits thermodynamic properties of compounds and liquid in the (LiF, NaF, KF, CrF₂)-CrF₃ systems by utilizing CALPHAD modeling with inputs from the DFT-based first-principles, phonon, and AIMD calculations. Thermodynamic properties, including enthalpy, entropy, and heat capacity of the binary (endmember) compounds LiF, NaF, KF, CrF₃, and CrF₂ as a function of temperature, have been predicted by DFT-based phonon calculations, agreeing with available experimental data in the literature and validating the reliability of the present methodology. They enabled the remodeling of the (LiF, NaF, KF, CrF₂)-CrF₃ systems with more accurate inputs. The MQMQA is employed to describe the liquid phase, providing valuable insights into the complex nature of molten salts such as the short-range ordering and neighboring of cations. Phase equilibria from the present CALPHAD modeling match better with experimental data in comparison with previous modeling work in the literature. The present thermodynamic data, including equilibrium volumes, bulk moduli, enthalpies, entropies, and heat capacities of compounds in the (LiF, NaF, KF, CrF₂)-CrF₃ system can be used to facilitate the development of advanced molten salt reactors.

Acknowledgments

The authors acknowledge financial supports by the U.S. Department of Energy, Office of Nuclear Energy's Nuclear Energy University Programs via Award Nos. DE-NE0008945 and DE-NE0009288. First-principles calculations were performed partially on the Roar supercomputer at the Pennsylvania State University's Institute for Computational and Data Sciences (ICDS), partially on the resources of the National Energy Research Scientific Computing Center (NERSC) supported by the U.S. Department of Energy, Office of Science User Facility operated under Contract No. DE-AC02-05CH11231, and partially on the resources of ACCESS (previously the Extreme Science and Engineering Discovery Environment, XSEDE) supported by National Science Foundation (NSF) with Grant No. ACI-1548562.

6 Figures and Figure Captions

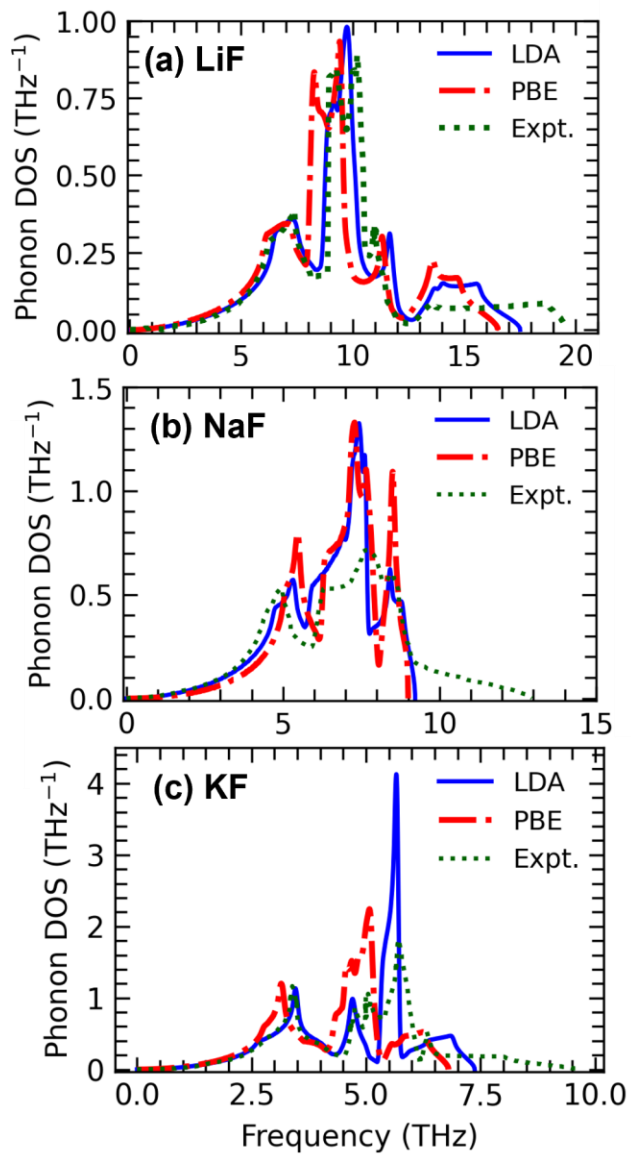


Figure 1. Predicted phonon density of states (DOS) of (a) LiF, (b) NaF, and (c) KF from DFT-based phonon calculations in comparison with phonon DOS from experiments [74–76]. Blue lines show results from the LDA approach, red dot-dashed lines show results from the GGA-PBE approach, and the green dotted lines are results from experiments [74–76].

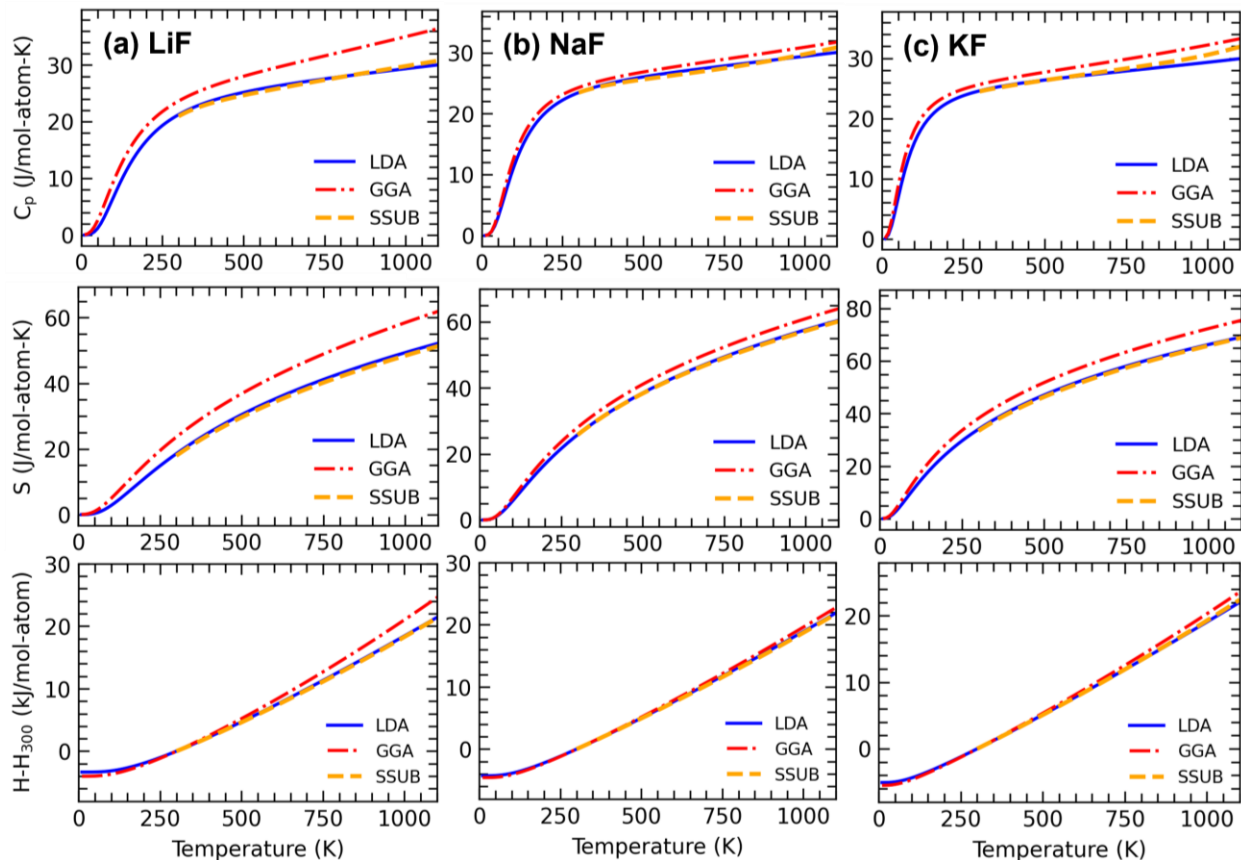


Figure 2. Predicted heat capacity C_p , entropy S , and enthalpy with reference at 300 K ($H-H_{300}$) of (a) LiF, (b) NaF, and (c) KF by DFT-based QHA via phonon calculations. Results by LDA is marked as solid blue lines, calculations by PBE are marked as dashed dot red lines, and the SSUB results [56] are in dashed yellow lines. The SSUB results are implemented in the present modeling work.

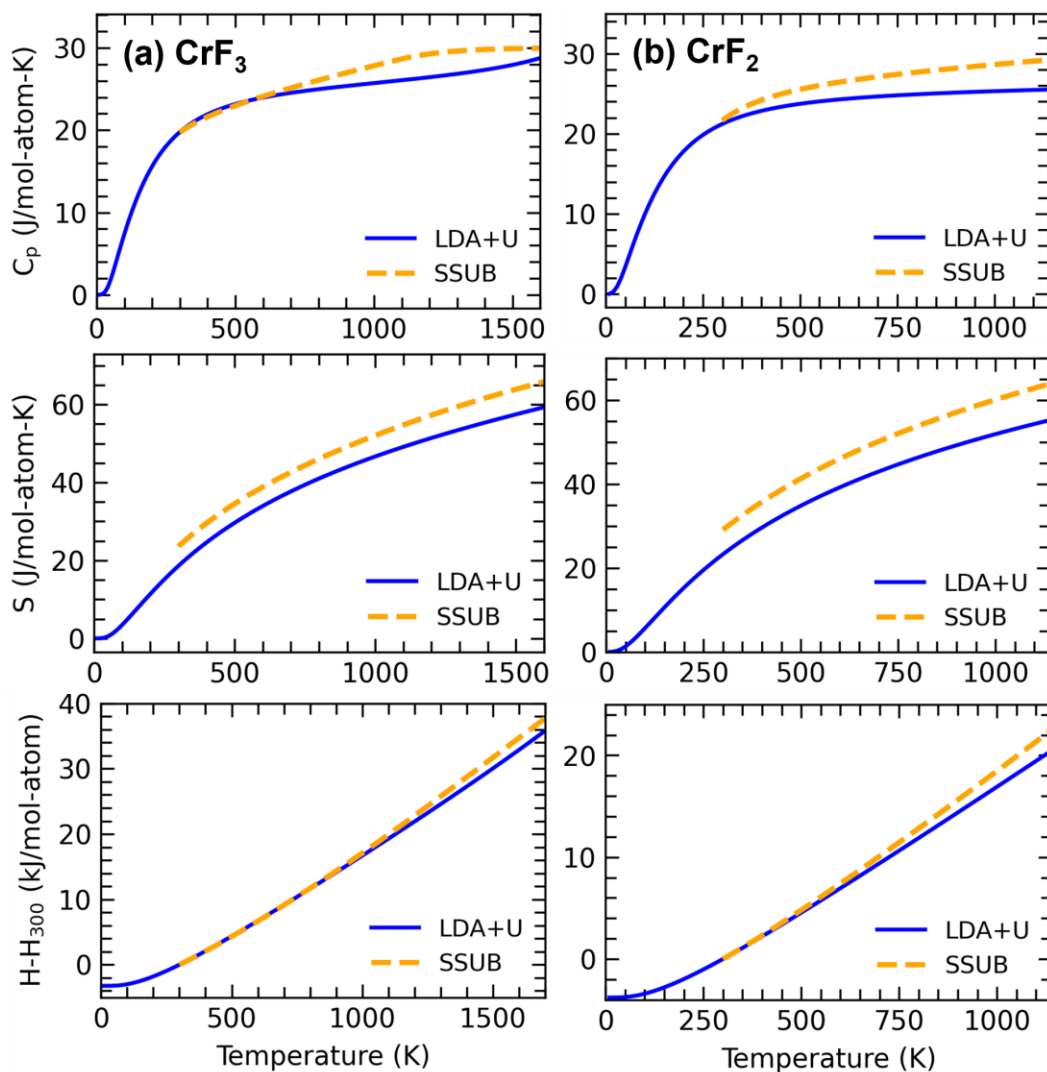


Figure 3. Predicted heat capacity C_p , entropy S , and enthalpy with reference at 300 K ($H-H_{300}$) of (a) CrF₃ and (b) CrF₂ by DFT-based QHA via phonon calculations marked in solid lines in comparison with SSUB [56] in dashed lines.

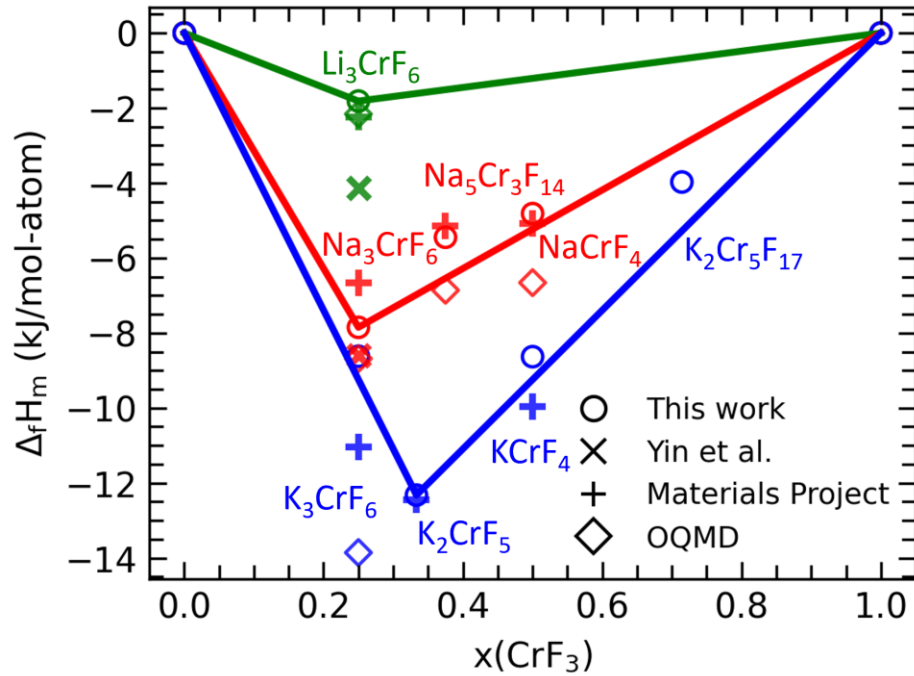


Figure 4. Convex hull of ternary compounds in LiF-CrF₃ (green), NaF-CrF₃ (red), and KF-CrF₃ (blue) at 0 K from DFT-based calculations from the present work. Circles (O) are formation enthalpy of compounds from the present work; cross markers (×) are formation enthalpy of compounds from Yin et al. [16,36]; plus markers (+) are results from The Materials Project [78]; and diamond markers (◇) are results from OQMD [79].

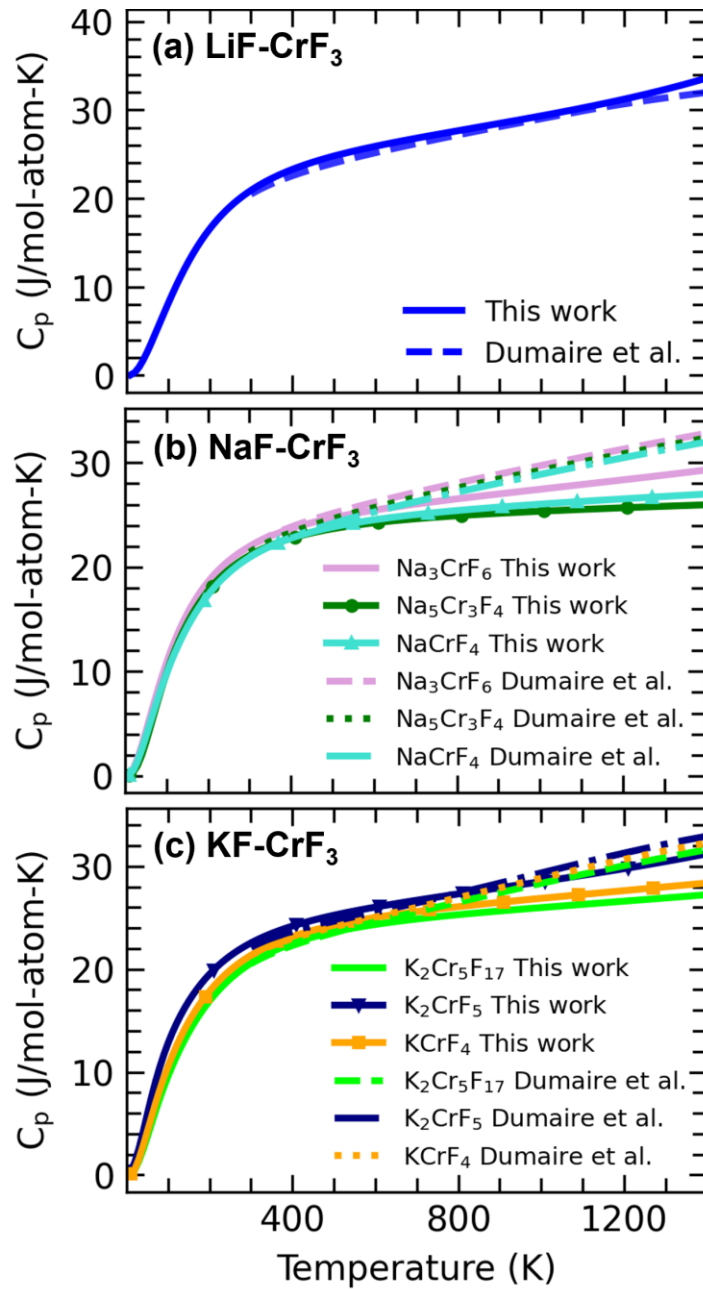


Figure 5. Predicted heat capacities of ternary compounds in the (a) LiF-CrF₃, (b) NaF-CrF₃, and (c) KF-CrF₃ systems by DFT-based QHA via phonon calculations (solid lines) compared with the Dumaire et al. [18]’s work (dashed lines). The QHA results are implemented in the present modeling work for ternary compounds.

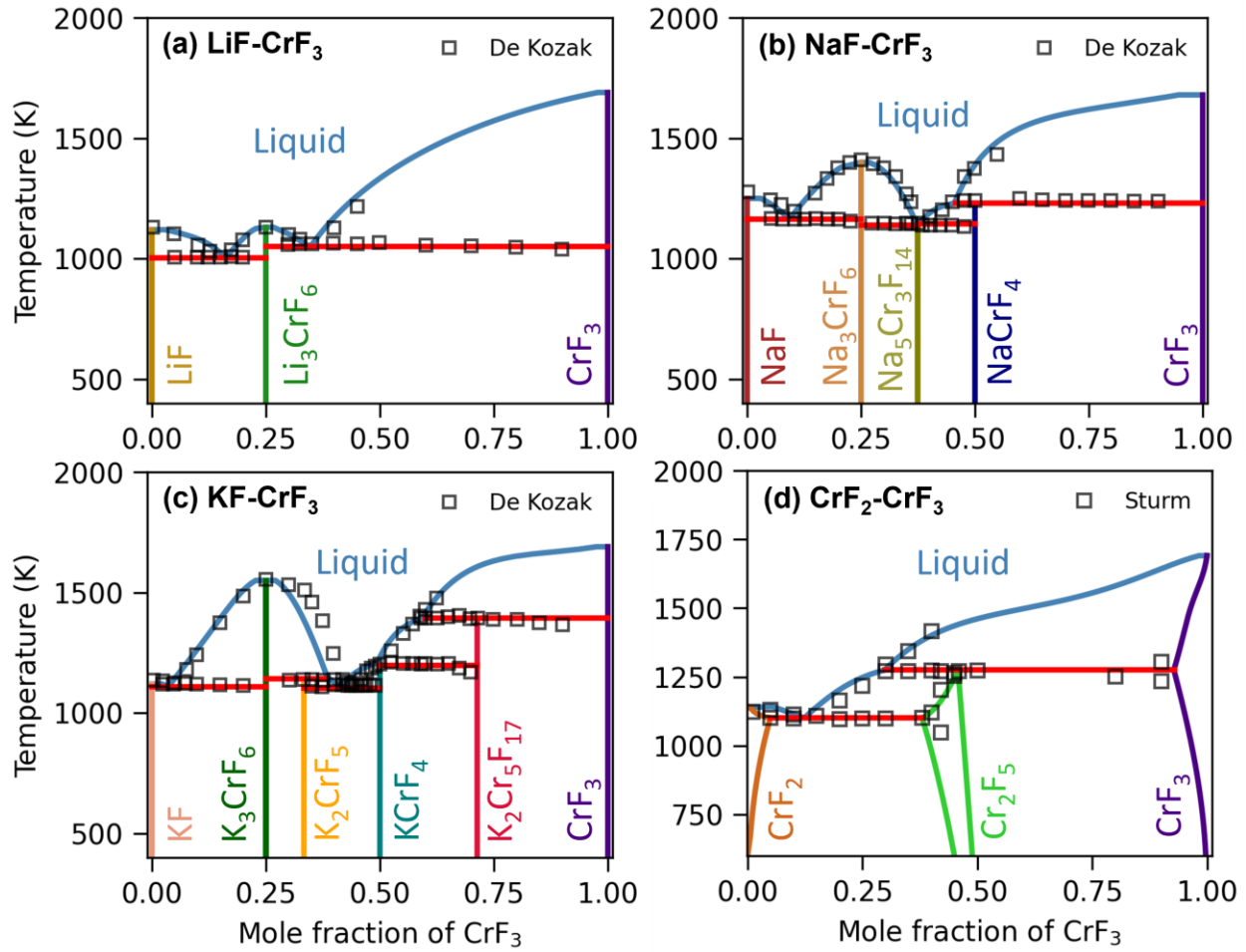


Figure 6. Predicted phase diagrams of the (a) LiF-CrF₃, (b) NaF-CrF₃, (c) KF-CrF₃, and (d) CrF₂-CrF₃ systems by the present CALPHAD modeling in comparison with experimental data [27,28,30].

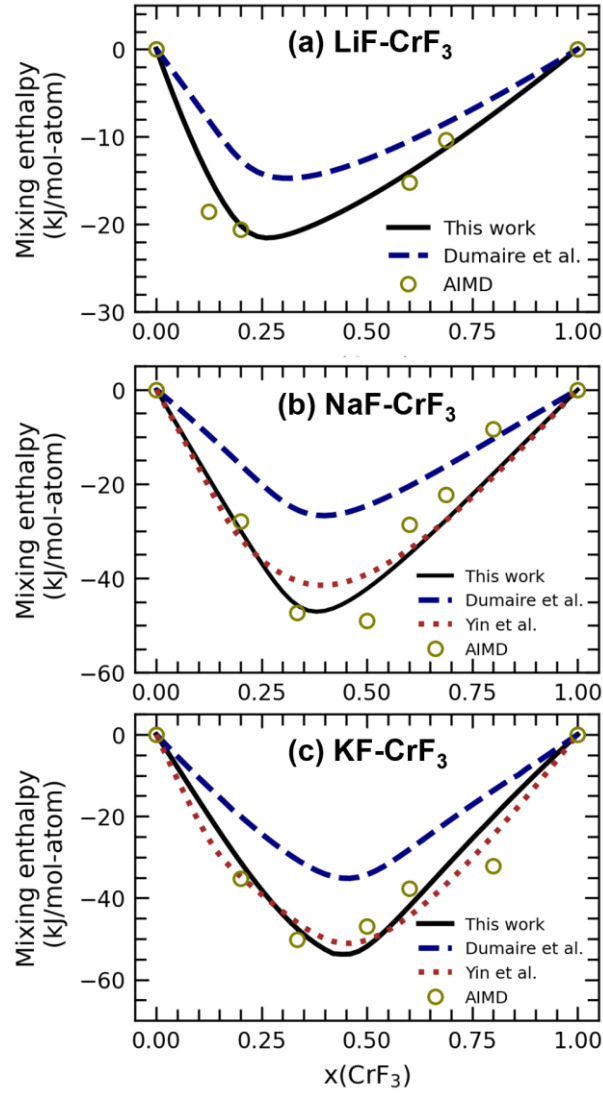


Figure 7. Predicted mixing enthalpy of liquid at 1700 K in (a) LiF-CrF₃, (b) NaF-CrF₃, and (c) KF-CrF₃ by the present CALPHAD modeling work (black solid lines), compared with the present AIMD results (circles) and modeling results by Dumaire et al. (blue dashed lines) [18] and Yin et al. (brown dotted lines) [16].

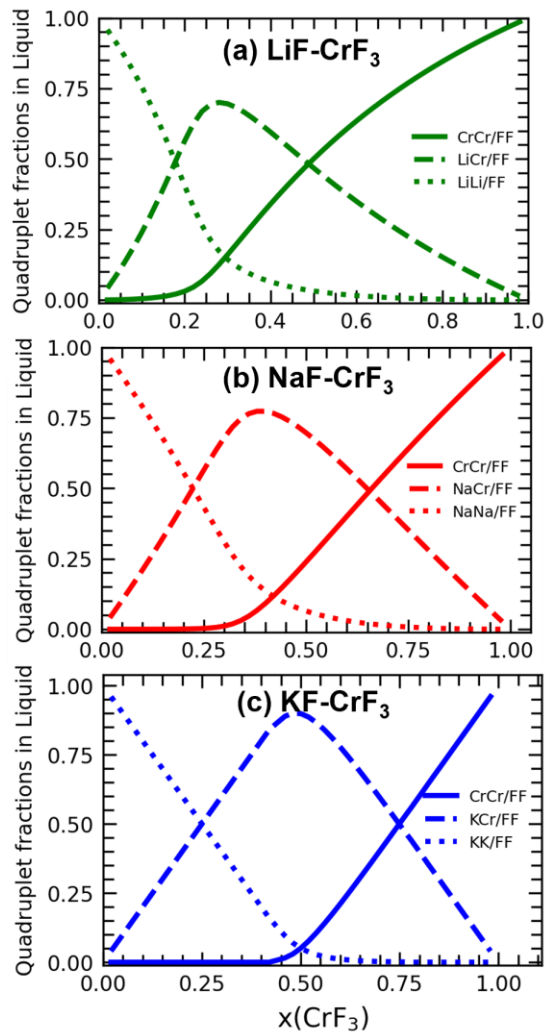


Figure 8. Predicted quadruplet fractions in (a) LiF-CrF₃ (green lines), (b) NaF-CrF₃ (red lines), and (c) KF-CrF₃ (blue lines) liquid at 1700 K according to the present CALPHAD modeling.

7 Tables and Table Captions

Table 1. Details of DFT-based first-principles, phonon, and AIMD simulations for each compound or phase, including space group, total atoms in the supercells, k-point meshes for structure relaxations and the final static calculations (indicated by DFT), supercell sizes for phonon calculations, k-point meshes for phonon calculations, and k-point meshes for AIMD calculations.

Phase	Space Group	Atoms in crystallographic cell	k-points for DFT	Atoms in supercell for phonon	k-points for phonon	k-points for AIMD
LiF	Fm $\bar{3}$ m	8	10 \times 10 \times 10	32	10 \times 10 \times 10	N/A
NaF	Fm $\bar{3}$ m	8	10 \times 10 \times 10	32	10 \times 10 \times 10	N/A
KF	Fm $\bar{3}$ m	8	10 \times 10 \times 10	32	10 \times 10 \times 10	N/A
CrF ₃	R $\bar{3}$ c	24	9 \times 9 \times 3	24	9 \times 9 \times 3	N/A
CrF ₂	P2 ₁ /c	6	14 \times 10 \times 9	24	13 \times 10 \times 9	N/A
Li ₃ CrF ₆	C2/c	60	2 \times 2 \times 2	60	2 \times 2 \times 2	N/A
Na ₃ CrF ₆	P2 ₁ /c	20	9 \times 8 \times 5	40	9 \times 8 \times 5	N/A
Na ₅ Cr ₃ F ₁₄	P2 ₁ /c	44	6 \times 6 \times 3	44	6 \times 6 \times 3	N/A
NaCrF ₄	P2 ₁ /c	24	6 \times 8 \times 5	24	6 \times 8 \times 6	N/A
K ₃ CrF ₆	Fm $\bar{3}$ m	40	5 \times 5 \times 5	40	5 \times 5 \times 5	N/A
K ₂ CrF ₅	Pbcn	128	3 \times 1 \times 1	128	3 \times 1 \times 1	N/A
KCrF ₄	Pnma	144	3 \times 1 \times 1	144	3 \times 1 \times 1	N/A
K ₂ Cr ₅ F ₁₇	Cmcm	96	2 \times 2 \times 2	96	2 \times 2 \times 2	N/A
Cr ₂ F ₅	C2/c	28	6 \times 6 \times 6	N/A	N/A	N/A
Liquid	N/A	108/128	N/A	N/A	N/A	1 \times 1 \times 1

Table 2. Coordination number used in the present CALPHAD modeling work with MQMQA for the liquid phase.

A	B	$Z_{AB:FF}^A$	$Z_{AB:FF}^B$	$Z_{AB:FF}^F$
Li ⁺	Li ⁺	6	6	6
Na ⁺	Na ⁺	6	6	6
K ⁺	K ⁺	6	6	6
Cr ³⁺	Cr ³⁺	6	6	2
Li ⁺	Cr ³⁺	2	6	2
Na ⁺	Cr ³⁺	4	6	2.7
K ⁺	Cr ³⁺	6	6	3
Cr ²⁺	Cr ³⁺	6	6	2.4
Cr ²⁺	Cr ²⁺	6	6	3

Table 3. Predicted equilibrium properties of volume V_0 , bulk modulus B_0 , and first derivative of bulk modulus with respect to pressure B' for each compound based on the present EOS fitting at 0 K (Eq. 2) in the FLiNaK-CrF₃-CrF₂ system. Experimental data (marked with *) [66–71] are also listed for comparison.

Phases	Method	V_0 (Å ³ /atom)	B_0 (GPa)	B'
LiF	LDA	7.488	86.5	4.25
	GGA	8.419	67.6	4.17
	Yagi* [66]		66.5	
	Hausühl* [67]		76.9	
	Boehler et al.* [68]		65.4	4.98

NaF	LDA	11.457	61.4	4.74
	GGA	13.020	45.0	4.60
	Yagi* [66]		45.9	
	Haussühl* [67]		53.8	
	Ramji Rao* [69]		52.3	
	Bensch et al.* [70]		48.2	5.89
KF	LDA	17.363	43.5	5.06
	GGA	20.050	28.9	4.84
	Yagi* [66]		37.0	
	Haussühl* [67]		35.5	
CrF ₃	LDA+U	11.152	46.2	8.46
	GGA+U	12.902	29.3	7.29
	Jørgensen et al.* [71]		29.2	10.3
CrF ₂	LDA+U	12.443	71.1	2.74
Li ₃ CrF ₆	LDA+U	9.543	56.1	5.85
Na ₃ CrF ₆	LDA+U	11.577	57.5	5.46
Na ₅ Cr ₃ F ₁₄	LDA+U	11.757	52.2	5.15
NaCrF ₄	LDA+U	11.933	53.0	4.35
K ₃ CrF ₆	LDA+U	15.705	51.5	5.67
K ₂ CrF ₅	LDA+U	13.858	45.9	5.65
KCrF ₄	LDA+U	13.920	38.1	4.88

K ₂ Cr ₅ F ₁₇	LDA+U	13.314	49.3	6.91
Cr ₂ F ₅	LDA+U	12.225	46.6	7.91

Table 4. Model parameters for excess Gibbs energy of the liquid phase in the (LiF, NaF, KF, CrF₂)-CrF₃ systems.

System	Parameter values
LiF-CrF ₃	$\Delta g_{\text{LiCr:F}_2}^{\text{ex}} = -31640.38 + 1.63T + (-13214.96 + 14.99T)\chi_{\text{LiCr/F}_2}$ $+ (-7028.37 + 2.00T)\chi_{\text{CrLi/F}_2} + (189.18$ $- 3.60T)\chi_{\text{CrLi/F}_2}^2$
NaF-CrF ₃	$\Delta g_{\text{NaCr:F}_2}^{\text{ex}} = -48031.37 + -3.06T + (-4558.94 - 21.26T)\chi_{\frac{\text{NaCr}}{\text{F}_2}}$ $+ (3537.07 + 5.49T)\chi_{\frac{\text{CrNa}}{\text{F}_2}} + 2000.00\chi_{\text{NaCr/F}_2}^2$
KF-CrF ₃	$\Delta g_{\text{LiCr:F}_2}^{\text{ex}} = -36789.86 - 35.26T + (5405.72 + 6.46T)\chi_{\text{KCr/F}_2}$ $+ (-39957.003 - 40.69T)\chi_{\text{CrK/F}_2} + (24251.79$ $+ 12.21T)\chi_{\text{CrK/F}_2}^2$
CrF ₂ -CrF ₃	$\Delta g_{\text{Cr}^{2+}\text{Cr}^{3+}:\text{F}_2}^{\text{ex}} = -9425.83 + 9.15T + (2931.90 - 15.29T)\chi_{\frac{\text{Cr}^{2+}\text{Cr}^{3+}}{\text{F}_2}}$ $+ (-6800.00 - 4.50T)\chi_{\text{Cr}^{3+}\text{Cr}^{2+}/\text{F}_2} + (6450.00$ $- 5.35T)\chi_{\text{Cr}^{2+}\text{Cr}^{3+}/\text{F}_2}^2$

Table 5. DFT-based results of formation enthalpy ($\Delta_f H_m$) at 0 K of ternary compounds in the AF-CrF₃ (A=Li, Na, and K) systems with the reference states as shown in the reactions. DFT results from Yin et al. [16,36], the Materials Project [78], and the Open Quantum Materials Database (OQMD) [79] are listed for comparison.

Compound	Reaction	$\Delta_f H_m$ (J/mol-atom)	Source
Li ₃ CrF ₆	Li ₃ CrF ₆ = 3LiF + CrF ₃	-1815	This work
		-4144	Yin et al.[36]
		-2238	Materials Project [78]
		-2161	OQMD [79]
Na ₃ CrF ₆	Na ₃ CrF ₆ = 3NaF + CrF ₃	-7849	This work
		-8592	Yin et al.[16]
		-6657	Materials Project [78]
		-8683	OQMD [79]
Na ₅ Cr ₃ F ₁₄	Na ₅ Cr ₃ F ₁₄ = 5NaF + 3CrF ₃	-5447	This work
		-5148	Materials Project [78]
		-6859	OQMD [79]
NaCrF ₄	NaCrF ₄ = NaF + CrF ₃	-4816	This work
		-5071	Materials Project [78]
		-6657	OQMD [79]
K ₃ CrF ₆	K ₃ CrF ₆ = 3KF + CrF ₃	-8621	This work
		-11038	Materials Project [78]
		-13855	OQMD [79]
K ₂ CrF ₅	K ₂ CrF ₅ = 2KF + CrF ₃	-12322	This work
		-12446	Materials Project [78]

KCrF ₄	KCrF ₄ = KF + CrF ₃	-8631	This work
		-9970	Materials Project [78]
K ₂ Cr ₅ F ₁₇	K ₂ Cr ₅ F ₁₇ = 2KF + 5CrF ₃	-3974	This work

Table 6. Predicted invariant equilibria in the AF-CrF₃ (A=Li, Na, K) systems by the present CALPHAD modeling, compared with experimental data from De Kozak [27] and Sturm [30] (marked with *), and other modeling works [16–18,36].

Reaction	x(CrF ₃)	Temperature (K)	Source	
Eutectic	Liquid↔LiF+Li ₃ CrF ₆	0.159	1004	This work
		0.150	1003	De Kozak [27] *
		0.136	1008	Dumaire et al.[18]
		0.148	1003	Yin et al.[36]
Congruent melting	Liquid↔Li ₃ CrF ₆	0.25	1134	This work
		0.25	1129	De Kozak [27] *
		0.25	1114	Hong et al.[64]
		0.25	1111	Dumaire et al.[18]
		0.25	1125	Yin et al.[36]
Eutectic	Liquid↔CrF ₃ + Li ₃ CrF ₆	0.345	1051	This work
		0.350	1059	De Kozak [27] *
		0.363	1062	Dumaire et al.[18]
		0.354	1058	Yin et al.[36]
Eutectic	Liquid↔NaF+Na ₃ CrF ₆	0.093	1164	This work
		0.123	1166	De Kozak [27] *
		0.106	1175	Dumaire et al.[18]

		0.114	1162	Yin et al.[16]
Congruent melting	Liquid \leftrightarrow Na ₃ CrF ₆	0.25	1403	This work
		0.25	1413	De Kozak [27] *
		0.25	1404	Hong et al.[64]
		0.25	1385	Dumaire et al.[18]
		0.25	1416	Yin et al.[16]
Eutectic	Liquid \leftrightarrow Na ₅ Cr ₃ F ₁₄ +Na ₃ CrF ₆	0.373	1139	This work
		0.371	1145	Dumaire et al.[18]
		0.367	1142	Yin et al.[16]
Eutectic	Liquid \leftrightarrow Na ₅ Cr ₃ F ₁₄ +NaCrF ₄	0.378	1144	This work
		0.381	1144	Dumaire et al.[18]
		0.383	1141	Yin et al.[16]
Peritectic	Liquid+CrF ₃ \leftrightarrow NaCrF ₄	0.5	1231	This work
		0.5	1234	De Kozak [27] *
		0.5	1232	Dumaire et al.[18]
		0.5	1239	Yin et al.[16]
Eutectic	Liquid \leftrightarrow KF+K ₃ CrF ₆	0.037	1110	This work
		0.048	1115	De Kozak [27] *
		0.041	1108	Dumaire et al.[18]
		0.045	1113	Yin et al.[17]
Congruent melting	Liquid \leftrightarrow K ₃ CrF ₆	0.25	1555	This work
		0.25	1553	De Kozak [27] *
		0.25	1520	Hong et al.[64]

		0.25	1553	Dumaire et al.[18]
		0.25	1548	Yin et al.[17]
Peritectic	Liquid+K ₃ CrF ₆ ↔K ₂ CrF ₅	0.333	1141	This work
		0.333	1133	De Kozak [27] *
		0.333	1130	Dumaire et al.[18]
		0.333	1135	Yin et al.[17]
Eutectic	Liquid↔KCrF ₄ +K ₂ CrF ₅	0.408	1103	This work
		0.45	1112	De Kozak [27] *
		0.432	1112	Dumaire et al.[18]
		0.426	1107	Yin et al.[17]
Peritectic	Liquid+K ₂ Cr ₅ F ₁₇ ↔KCrF ₄	0.5	1194	This work
		0.5	1200	De Kozak [27] *
		0.5	1191	Dumaire et al.[18]
		0.5	1195	Yin et al.[17]
Peritectic	Liquid+CrF ₃ ↔K ₂ Cr ₅ F ₁₇	0.714	1394	This work
		0.714	1390	De Kozak [27] *
		0.714	1390	Dumaire et al.[18]
		0.714	1388	Yin et al.[17]
Eutectic	Liquid↔CrF ₂ +Cr ₂ F ₅	0.124	1101	This work
		0.14	1103	Sturm [30] *
		0.115	1104	Dumaire et al.[18]
Peritectic	Liquid+CrF ₃ ↔Cr ₂ F ₅	0.299	1276	This work
		0.29	1272	Sturm [30] *

0.28

1271

Dumaire et al.[18]

8 References

- [1] Oak Ridge National Laboratory, Molten Salt Chemistry Workshop, 2017. https://www.mendeley.com/catalogue/a7161e57-11e6-3d48-ad7b-7ea7e8e78b7e/?utm_source=desktop&utm_medium=1.19.8&utm_campaign=open_catalog&userDocumentId=%7Bfc60b448-59fe-4956-99a7-10a98b9c87d1%7D (accessed April 28, 2023).
- [2] T. Abram, S. Ion, Generation-IV nuclear power: A review of the state of the science, *Energy Policy*. 36 (2008) 4323–4330. <https://doi.org/10.1016/J.ENPOL.2008.09.059>.
- [3] W. Cottrell, Operation of the Aircraft Reactor Experiment, 1959. <https://books.google.com/books?hl=en&lr=&id=AK6iQSWmp8sC&oi=fnd&pg=PA1&dq=Cottrell,+W.+B.%3B+et+al.%3B+Operation+of+the+aircraft+reactor+experiment%3B+Oak+Ridge,+1955.&ots=1FE1wYZ2zA&sig=OaS2dh6ix-KnSoNHgIfh-3n6idI> (accessed May 1, 2023).
- [4] D. LeBlanc, Molten salt reactors: A new beginning for an old idea, *Nucl. Eng. Des.* 240 (2010) 1644–1656. <https://doi.org/10.1016/J.NUCENGDES.2009.12.033>.
- [5] O. Beneš, R.J.M. Konings, Thermodynamic Calculations of Molten-Salt Reactor Fuel Systems, in: *Molten Salts Chem.*, Elsevier, 2013: pp. 49–78. <https://doi.org/10.1016/B978-0-12-398538-5.00004-4>.
- [6] A.G. Bergman, E.P. Dergunov, *Ann. N.Y. Acad. Sci.*, U.R.S.S. 31 (1941) 753. <https://scholar.google.com/scholar?inst=15460120341296470254&q=A.G.+Bergman+and+E.P.+Dergunov%2C+Verg.+Compt.+Rend.+Acad.+Sci.%2C+U.R.S.S.%2C31%2C+753+%281941%29>. (accessed November 16, 2023).
- [7] J.A. Lane, Chemical Aspects of Molten-Fluoride-Salt Reactor Fuels, *Fluid Fuel React.* (1958) 569–594.
- [8] J.W. Koger, Evaluation of Hastelloy N alloys after nine years exposure to both a molten fluoride salt and air at temperatures from 700 to 560 C, (1972). <https://doi.org/10.2172/4468052>.
- [9] W.D. Manly, J.H. Coobs, J.H. DeVan, D.A. Douglas, H. Inouye, P. Partiarca, T.K. Roche, J.L. Scott, Metallurgical problems in molten fluoride systems, (1958). <https://www.osti.gov/biblio/4308214> (accessed May 1, 2023).
- [10] L.C. Olson, J.W. Ambrosek, K. Sridharan, M.H. Anderson, T.R. Allen, Materials corrosion in molten LiF–NaF–KF salt, *J. Fluor. Chem.* 130 (2009) 67–73. <https://doi.org/10.1016/J.JFLUCHEM.2008.05.008>.
- [11] F.Y. Ouyang, C.H. Chang, J.J. Kai, Long-term corrosion behaviors of Hastelloy-N and Hastelloy-B3 in moisture-containing molten FLiNaK salt environments, *J. Nucl. Mater.* 446 (2014) 81–89. <https://doi.org/10.1016/J.JNUCMAT.2013.11.045>.
- [12] Y. Liu, Y. Song, H. Ai, M. Shen, H. Liu, S. Zhao, Y. Liu, Z. Fei, X. Fu, J. Cheng, Corrosion of Cr in molten salts with different fluoroacidity in the presence of CrF₃, *Corros. Sci.* 169 (2020) 108636. <https://doi.org/10.1016/J.CORSCI.2020.108636>.
- [13] P. Chartrand, A.D. Pelton, Thermodynamic evaluation and optimization of the LiF–NaF–

- KF-MgF₂-CaF₂ system using the modified quasi-chemical model, *Metall. Mater. Trans. A Phys. Metall. Mater. Sci.* 32 (2001) 1385–1396. <https://doi.org/10.1007/s11661-001-0228-1>.
- [14] K. Wang, J.H. Cheng, P. Zhang, Y. Zuo, L.D. Xie, Phase diagram calculations of the LiF-NaF-KF system, *Beijing Keji Daxue Xuebao/Journal Univ. Sci. Technol. Beijing.* 36 (2014) 1666–1675. <https://doi.org/10.13374/j.issn1001-053x.2014.12.014>.
- [15] J.C. Ard, J.A. Yingling, K.E. Johnson, J. Schorne-Pinto, M. Aziziha, C.M. Dixon, M.S. Christian, J.W. McMurray, T.M. Besmann, Development of the Molten Salt Thermal Properties Database – Thermochemical (MSTDB–TC), example applications, and LiCl–RbCl and UF₃–UF₄ system assessments, *J. Nucl. Mater.* 563 (2022) 153631. <https://doi.org/10.1016/j.jnucmat.2022.153631>.
- [16] H. Yin, P. Zhang, X. An, J. Cheng, X. Li, S. Wu, X. Wu, W. Liu, L. Xie, Thermodynamic modeling of LiF-NaF-KF-CrF₃ system, *J. Fluor. Chem.* 209 (2018) 6–13. <https://doi.org/10.1016/J.JFLUCHEM.2018.02.005>.
- [17] H. Yin, K. Wang, L. Xie, H. Han, W. Wang, Thermodynamic modeling of KF-CrF₃ binary system, *Chem. Res. Chinese Univ.* 31 (2015) 461–465. <https://doi.org/10.1007/s40242-015-4319-8>.
- [18] T. Dumaire, R.J.M. Konings, A.L. Smith, Thermodynamic Assessment of the AF–CrF₃ (A = Li, Na, K) and CrF₂–CrF₃ Systems, *Thermo.* 1 (2021) 205–219. <https://doi.org/10.3390/thermo1020014>.
- [19] Z.K. Liu, Computational thermodynamics and its applications, *Acta Mater.* 200 (2020) 745–792. <https://doi.org/10.1016/J.ACTAMAT.2020.08.008>.
- [20] Z.-K. Liu, Y. Wang, Computational thermodynamics of materials, Cambridge University Press, 2016.
- [21] L. Kaufman, H. Bernstein, Computer calculation of phase diagrams. With special reference to refractory metals, 1970.
- [22] A.D. Pelton, P. Chartrand, G. Eriksson, The modified quasi-chemical model: Part IV. Two-sublattice quadruplet approximation, *Metall. Mater. Trans. A Phys. Metall. Mater. Sci.* 32 (2001) 1409–1416.
- [23] B. Bocklund, R. Otis, A. Egorov, A. Obaied, I. Roslyakova, Z.K. Liu, ESPEI for efficient thermodynamic database development, modification, and uncertainty quantification: Application to Cu-Mg, *MRS Commun.* 9 (2019) 618–627. <https://doi.org/10.1557/mrc.2019.59>.
- [24] ESPEI, (n.d.). <https://espei.org/en/latest/>.
- [25] R. Otis, Z.-K. Liu, pycalphad: CALPHAD-based Computational Thermodynamics in Python, *J. Open Res. Softw.* 5 (2017) 1–11. <https://doi.org/10.5334/jors.140>.
- [26] pycalphad, (n.d.). <https://pycalphad.org/docs/latest/> (accessed February 15, 2024).
- [27] A. De Kozak, Les systèmes CrF₃–MF (M = Li, Na ou K), *C. R. Acad. Sci. Paris.* (1969) 416–418.
- [28] A. de Kozak, M. Samouël, Le système ternaire NaF-ZnF₂-CrF₃. I. étude radiocristallographique. Triangulation, *J. Less-Common Met.* 40 (1975) 185–193. [https://doi.org/10.1016/0022-5088\(75\)90060-0](https://doi.org/10.1016/0022-5088(75)90060-0).
- [29] J.-P. Miranday, G. Ferey, C. Jacoboni, J.-M. Dance, A. Tressaud, R. De Pape, Croissance

- cristalline, polymorphisme et propriétés magnétiques de Na₅Cr₃F₁₄, Hal.Science. (n.d.). <https://hal.science/hal-00131293/document> (accessed May 3, 2023).
- [30] B.J. Sturm, Phase Equilibria in the System Chromium(II) Fluoride-Chromium(III) Fluoride, *Inorg. Chem.* 1 (1962) 665–672. https://doi.org/10.1021/IC50003A043/ASSET/IC50003A043.FP.PNG_V03.
- [31] P. García-Fernández, M. Moreno, J.A. Aramburu, Electrostatic control of orbital ordering in noncubic crystals, *J. Phys. Chem. C.* 118 (2014) 7554–7561. https://doi.org/10.1021/JP412329X/SUPPL_FILE/JP412329X_SI_001.PDF.
- [32] G. Brunton, The crystal structure of Na₃CrF₆, *Mater. Res. Bull.* 4 (1969) 621–626. [https://doi.org/10.1016/0025-5408\(69\)90071-3](https://doi.org/10.1016/0025-5408(69)90071-3).
- [33] A. Le Bail, A.-M. Mercier, Distorted chiolite crystal structures of α -Na₅M₃F₁₄ (M=Cr,Fe,Ga) studied by X-ray powder diffraction, *Powder Diffr.* 18 (2003) 128–134. <https://doi.org/10.1154/1.1556990>.
- [34] H. Manaka, T. Etoh, Y. Honda, N. Iwashita, K. Ogata, N. Terada, T. Hisamatsu, M. Ito, Y. Narumi, A. Kondo, K. Kindo, Y. Miura, Effects of Geometrical Spin Frustration on Triangular Spin Tubes Formed in CsCrF₄ and α -KCrF₄, <Http://Dx.Doi.Org/10.1143/JPSJ.80.084714>. 80 (2011). <https://doi.org/10.1143/JPSJ.80.084714>.
- [35] C. Sassoie, A. De Kozak, Crystal Structure and Thermal Behaviour of K₂[CrF₅·H₂O], *Zeitschrift Für Anorg. Und Allg. Chemie.* 632 (2006) 445–448. <https://doi.org/10.1002/ZAAC.200500458>.
- [36] H. Yin, K. Wang, W. Liu, L. Xie, H. Han, W. Wang, Thermodynamic modeling of the LiF-CrF₃ binary system, *Gaodeng Xuexiao Huaxue Xuebao/Chemical J. Chinese Univ.* 35 (2014) 2668–2673. <https://doi.org/10.7503/CJCU20140396>.
- [37] J. Leitner, P. Voňka, D. Sedmidubský, P. Svoboda, Application of Neumann-Kopp rule for the estimation of heat capacity of mixed oxides, *Thermochim. Acta.* 497 (2010) 7–13. <https://doi.org/10.1016/j.tca.2009.08.002>.
- [38] S.L. Shang, Y. Wang, D.E. Kim, Z.K. Liu, First-principles thermodynamics from phonon and Debye model: Application to Ni and Ni₃Al, *Comput. Mater. Sci.* 47 (2010) 1040–1048. <https://doi.org/10.1016/j.commatsci.2009.12.006>.
- [39] Y. Wang, Z.K. Liu, L.Q. Chen, Thermodynamic properties of Al, Ni, NiAl, and Ni₃Al from first-principles calculations, *Acta Mater.* 52 (2004) 2665–2671. <https://doi.org/10.1016/j.actamat.2004.02.014>.
- [40] A. Van de Walle, G. Ceder, The effect of lattice vibrations on substitutional alloy thermodynamics, *Rev. Mod. Phys.* 74 (2002) 11–45. <https://doi.org/10.1103/RevModPhys.74.11>.
- [41] G. Kresse, J. Furthmuller, J. Furthmüller, J. Furthmuller, J. Furthmüller, J. Furthmueller, J. Furthmuller, J. Furthmüller, Efficient iterative schemes for ab initio total-energy calculations using a plane-wave basis set, *Phys. Rev. B-Condensed Matter.* 54 (1996) 11169–11186. <https://doi.org/10.1103/PhysRevB.54.11169>.
- [42] P.E. Blöchl, Projector augmented-wave method, *Phys. Rev. B.* 50 (1994) 17953–17979. <https://doi.org/10.1103/PhysRevB.50.17953>.
- [43] D. Joubert, From ultrasoft pseudopotentials to the projector augmented-wave method,

- Phys. Rev. B - Condens. Matter Mater. Phys. 59 (1999) 1758–1775.
<https://doi.org/10.1103/PhysRevB.59.1758>.
- [44] J.P. Perdew, A. Zunger, Self-interaction correction to density-functional approximations for many-electron systems, *Phys. Rev. B.* 23 (1981) 5048–5079.
<https://doi.org/10.1103/PhysRevB.23.5048>.
- [45] J.P. Perdew, K. Burke, M. Ernzerhof, Generalized gradient approximation made simple, *Phys. Rev. Lett.* 77 (1996) 3865–3868. <https://doi.org/10.1103/PhysRevLett.77.3865>.
- [46] S. Shi, A.L. Wysocki, K.D. Belashchenko, Magnetism of chromia from first-principles calculations, *Phys. Rev. B - Condens. Matter Mater. Phys.* 79 (2009) 104404.
<https://doi.org/10.1103/PHYSREVB.79.104404>/FIGURES/3/MEDIUM.
- [47] S. Mattsson, B. Paulus, Density Functional Theory Calculations of Structural, Electronic, and Magnetic Properties of the 3d Metal Trifluorides MF₃ (M = Ti-Ni) in the Solid State, *J. Comput. Chem.* 40 (2019) 1190–1197. <https://doi.org/10.1002/jcc.25777>.
- [48] X. Huang, P.C.M. Fossati, L. Martinelli, S. Bosonnet, L. Latu-Romain, Y. Wouters, A DFT study of defects in paramagnetic Cr₂O₃, *Phys. Chem. Chem. Phys.* 24 (2022) 10488–10498. <https://doi.org/10.1039/D1CP05756A>.
- [49] A. van de Walle, Multicomponent multisublattice alloys, nonconfigurational entropy and other additions to the Alloy Theoretic Automated Toolkit, *Calphad Comput. Coupling Phase Diagrams Thermochem.* 33 (2009) 266–278.
<https://doi.org/10.1016/j.calphad.2008.12.005>.
- [50] Y. Wang, M. Liao, B.J. Bocklund, P. Gao, S.L. Shang, H. Kim, A.M. Beese, L.Q. Chen, Z.K. Liu, DFTTK: Density Functional Theory ToolKit for high-throughput lattice dynamics calculations, *Calphad.* 75 (2021) 102355.
<https://doi.org/10.1016/J.CALPHAD.2021.102355>.
- [51] Y. Wang, L.Q. Chen, Z.K. Liu, YPHON: A package for calculating phonons of polar materials, *Comput. Phys. Commun.* 185 (2014) 2950–2968.
<https://doi.org/10.1016/j.cpc.2014.06.023>.
- [52] S. Nosé, A unified formulation of the constant temperature molecular dynamics methods, *J. Chem. Phys.* 81 (1984) 511–519. <https://doi.org/10.1063/1.447334>.
- [53] R.J.M. Konings, R.E. Stoller, *Comprehensive Nuclear Materials*, Compr. Nucl. Mater. Second Ed. (2020) 1–4653. <https://doi.org/10.1016/c2017-1-02873-8>.
- [54] M.W. Chase, J.L. Curnutt, J.R. Downey, R.A. McDonald, A.N. Syverud, E.A. Valenzuela, JANAF Thermochemical Tables, 1982 Supplement, *J. Phys. Chem. Ref. Data.* 11 (2009) 695. <https://doi.org/10.1063/1.555666>.
- [55] L. V Gurvich, V.S. Iorish, D. V Chekhovskoi, V.S. Yungman, IVTANTHERMO—a thermodynamic database and software system for the personal computer, *NIST Spec. Database.* 5 (1993).
- [56] SGTE Substance Database - SGTE - Scientific Group Thermodata Europe, (n.d).
<https://www.sgte.net/en/neu>.
- [57] A.D. Pelton, S.A. Degterov, G. Eriksson, C. Robelin, Y. Dessureault, The modified quasichemical model I - Binary solutions, *Metall. Mater. Trans. B Process Metall. Mater. Process. Sci.* 31 (2000) 651–659. <https://doi.org/10.1007/s11663-000-0103-2>.
- [58] A.D. Pelton, P. Chartrand, G. Eriksson, The modified quasi-chemical model: Part IV.

- Two-sublattice quadruplet approximation, *Metall. Mater. Trans. A* 2001 326. 32 (2001) 1409–1416. <https://doi.org/10.1007/S11661-001-0230-7>.
- [59] F. Kohler, Estimation of the thermodynamic data for a ternary system from the corresponding binary systems, *Monatsh. Chem.* 91 (1960) 738–760. https://scholar.google.com/scholar?hl=en&as_sdt=0%2C39&inst=15460120341296470254&q=Estimation+of+the+thermodynamic+data+for+a+ternary+system+from+the+corresponding+binary+systems%2C+Monatsh.+Chem.%2C+1960%2C+91%2C+738-740.+&btnG= (accessed November 16, 2023).
- [60] G.W. Toop, Predicting Ternary Activities Using Binary Data, *Trans. TMS-AIME.* 223 (1965) 850–855. <https://doi.org/10.1252/JCEJ.40.295>.
- [61] P. Chartrand, A.D. Pelton, On the choice of “geometric” thermodynamic models patrice chartrand and arthur D. Pelton, *J. Phase Equilibria.* 21 (2000) 141–147. <https://doi.org/10.1361/105497100770340192/METRICS>.
- [62] A.D. Pelton, A general “geometric” thermodynamic model for multicomponent solutions, *Calphad.* 25 (2001) 319–328. [https://doi.org/10.1016/S0364-5916\(01\)00052-9](https://doi.org/10.1016/S0364-5916(01)00052-9).
- [63] O. Redlich, A.T. Kister, Algebraic Representation of Thermodynamic Properties and the Classification of Solutions, *Ind. Eng. Chem.* 40 (1948) 345–348. <https://doi.org/10.1021/ie50458a036>.
- [64] Q.J. Hong, S. V. Ushakov, A. van de Walle, A. Navrotsky, Melting temperature prediction using a graph neural network model: From ancient minerals to new materials, *Proc. Natl. Acad. Sci. U. S. A.* 119 (2022) e2209630119. https://doi.org/10.1073/PNAS.2209630119/SUPPL_FILE/PNAS.2209630119.SD02.XLSX.
- [65] J. Paz Soldan Palma, R. Gong, B.J. Bocklund, R. Otis, M. Poschmann, M. Piro, S. Shahbazi, T.G. Levitskaia, S. Hu, N.D. Smith, Y. Wang, H. Kim, Z.-K. Liu, S.-L. Shang, Thermodynamic modeling with uncertainty quantification using the modified quasichemical model in quadruplet approximation: Implementation into PyCalphad and ESPEI, *Calphad.* 83 (2023) 102618. <https://doi.org/10.1016/j.calphad.2023.102618>.
- [66] T. Yagi, Experimental determination of thermal expansivity of several alkali halides at high pressures, *J. Phys. Chem. Solids.* 39 (1978) 563–571. [https://doi.org/10.1016/0022-3697\(78\)90037-9](https://doi.org/10.1016/0022-3697(78)90037-9).
- [67] S. Haussühl, Thermo-elastische Konstanten der Alkalihalogenide vom NaCl-Typ, *Zeitschrift Für Phys.* 159 (1960) 223–229. <https://doi.org/10.1007/BF01338349/METRICS>.
- [68] R. Boehler, G.C. Kennedy, Thermal expansion of LiF at high pressures, *J. Phys. Chem. Solids.* 41 (1980) 1019–1022. [https://doi.org/10.1016/0022-3697\(80\)90053-0](https://doi.org/10.1016/0022-3697(80)90053-0).
- [69] R. Ramji Rao, Anderson-Grüneisen parameter δ and the temperature dependence of the bulk modulus of some fluorides, *Physica.* 77 (1974) 126–130. [https://doi.org/10.1016/0031-8914\(74\)90280-8](https://doi.org/10.1016/0031-8914(74)90280-8).
- [70] W.A. Bensch, Third-Order Elastic Constants of NaF, *Phys. Rev. B.* 6 (1972) 1504. <https://doi.org/10.1103/PhysRevB.6.1504>.
- [71] J.E. Jørgensen, W.G. Marshall, R.I. Smith, The compression mechanism of CrF₃, *Acta Crystallogr. Sect. B Struct. Sci.* 60 (2004) 669–673.

- <https://doi.org/10.1107/S010876810402316X/CK50048SUP9.TXT>.
- [72] P. Haas, F. Tran, P. Blaha, Calculation of the lattice constant of solids with semilocal functionals, *Phys. Rev. B - Condens. Matter Mater. Phys.* 79 (2009) 085104. <https://doi.org/10.1103/PHYSREVB.79.085104/FIGURES/3/MEDIUM>.
- [73] L. He, F. Liu, G. Hautier, M.J.T. Oliveira, M.A.L. Marques, F.D. Vila, J.J. Rehr, G.M. Rignanese, A. Zhou, Accuracy of generalized gradient approximation functionals for density-functional perturbation theory calculations, *Phys. Rev. B - Condens. Matter Mater. Phys.* 89 (2014) 064305. <https://doi.org/10.1103/PHYSREVB.89.064305/FIGURES/11/MEDIUM>.
- [74] G. Dolling, H.G. Smith, R.M. Nicklow, P.R. Vijayaraghavan, M.K. Wilkinson, Lattice Dynamics of Lithium Fluoride, *Phys. Rev.* 168 (1968) 970–979. <https://doi.org/10.1103/PhysRev.168.970>.
- [75] W. Bührer, Lattice Dynamics of Potassium Fluoride, *Phys. Status Solidi.* 41 (1970) 789–795. <https://doi.org/10.1002/PSSB.19700410235>.
- [76] A.M. Karo, J.R. Hardy, Lattice Dynamics of NaF, *Phys. Rev.* 181 (1969) 1272–1277. <https://doi.org/10.1103/PhysRev.181.1272>.
- [77] S.L. Shang, Y. Wang, T.J. Anderson, Z.K. Liu, Achieving accurate energetics beyond (semi-)local density functional theory: Illustrated with transition metal disulfides, Cu₂ZnSnS₄, and Na₃PS₄ related semiconductors, *Phys. Rev. Mater.* 3 (2019) 1–11. <https://doi.org/10.1103/PhysRevMaterials.3.015401>.
- [78] A. Jain, S.P. Ong, G. Hautier, W. Chen, W.D. Richards, S. Dacek, S. Cholia, D. Gunter, D. Skinner, G. Ceder, K.A. Persson, Commentary: The materials project: A materials genome approach to accelerating materials innovation, *APL Mater.* 1 (2013) 11002. <https://doi.org/10.1063/1.4812323/119685>.
- [79] S. Kirklin, J.E. Saal, B. Meredig, A. Thompson, J.W. Doak, M. Aykol, S. Rühl, C. Wolverton, The Open Quantum Materials Database (OQMD): assessing the accuracy of DFT formation energies, *Npj Comput. Mater.* 2015 11. 1 (2015) 1–15. <https://doi.org/10.1038/npjcompumats.2015.10>.
- [80] C. Robelin, P. Chartrand, Thermodynamic evaluation and optimization of the (NaCl + KCl + MgCl₂ + CaCl₂ + ZnCl₂) system, *J. Chem. Thermodyn.* 43 (2011) 377–391. <https://doi.org/10.1016/j.jct.2010.10.013>.
- [81] A.D. Pelton, *Phase diagrams and thermodynamic modeling of solutions*, Elsevier, 2014.